

Have greenhouse gases intensified the contrast between wet and dry regions?

Article

Accepted Version

article

Polson, D., Hegerl, G. C., Allan, R. ORCID:
<https://orcid.org/0000-0003-0264-9447> and Balan Sarojini, B.
(2013) Have greenhouse gases intensified the contrast
between wet and dry regions? *Geophysical Research Letters*,
40 (17). pp. 4783-4787. ISSN 0094-8276 doi:
<https://doi.org/10.1002/grl.50923> Available at
<https://centaur.reading.ac.uk/34442/>

It is advisable to refer to the publisher's version if you intend to cite from the work. See [Guidance on citing](#).

Published version at: <http://dx.doi.org/10.1002/grl.50923>

To link to this article DOI: <http://dx.doi.org/10.1002/grl.50923>

Publisher: American Geophysical Union

All outputs in CentAUR are protected by Intellectual Property Rights law, including copyright law. Copyright and IPR is retained by the creators or other copyright holders. Terms and conditions for use of this material are defined in the [End User Agreement](#).

www.reading.ac.uk/centaur

CentAUR

Central Archive at the University of Reading

Reading's research outputs online

Auxiliary material for:

Have greenhouse gases intensified the contrast between wet and dry regions?

Geophysical Research Letters

D. Polson, G.C. Hegerl, R.P. Allan, and B. Balan Sarojini

The supplementary material shows results from the main paper for seasons not included there, results for land only and ocean only and illustrates the robustness of the results to the removal of ENSO, the observational dataset, method of defining the wet and dry regions and results for the wet and dry regions separately. It also provides some background technical details on the removal of the influence of ENSO from the observational precipitation data and choice of seasons.

a. Annual cycle of observed precipitation and influence of ENSO

Figure S1(a) shows the monthly tropical precipitation averaged over all years for the GPCP dataset in the Northern and Southern Hemispheres. The seasons January, February and March (JFM), April, May June (AMJ), July, August and September (JAS) and October, November and December (OND) where chosen to capture the wettest and driest seasons in each hemisphere. Figure S1(b) shows the HadCRUT4 annual global mean near surface temperature anomalies during the observation period (Morice et al. 2012).

As the record is short, trends will be influenced by ENSO. The influence of ENSO is removed from the observations in each gridbox by regressing the detrended MEI index (*Wolter and Timlin* 2011) onto detrended precipitation and subtracting the influence of ENSO from the observations in gridboxes where its influence was found to be significant (i.e. p-value

26 ≤ 0.05) using the Mann-Whitney test (*Kenyon and Hegerl 2010*). Averaging across the
27 simulations should largely remove the influence of ENSO in the multi-model mean as ENSO
28 events occur at random times in the simulations.

29 Figure S2 shows the timeseries for the Northern and Southern Hemisphere tropical and
30 subtropical dry and wet region precipitation without removing the influence of ENSO, while
31 Figure S3 shows the timeseries with the influence of ENSO removed. To ensure OND is
32 consistent with JFM, the OND data is from the previous year is 1987 to 2009. *Gu et al.*
33 (2007) show that the impact of volcanoes and ENSO on precipitation can be compounded.
34 To distinguish the two, the removal of ENSO was repeated with the years 1991, 1992 and
35 1993 (defined as volcanic years by *Gu et al. (2007)*) excluded from the regression of ENSO
36 onto the observations. The precipitation changes were not sensitive to treating the volcanic
37 years separately.

38 *b. Observed and modeled dry and wet regions*

39 Figures S4 and S5 show the locations of the GPCP dry and wet regions respectively,
40 when defined using method 1. Figures S6 and S7 show the locations of the GPCP dry and
41 wet regions when defined using method 2, which allows the size of the regions to change
42 over time. One change worth noting, is the dry regions tending to occur more often over
43 the NH eastern Pacific in the last 10 years of observations. This is consistent with studies
44 showing an intensification of the Walker circulation in the tropical Pacific in recent decades
45 (*Merrifield 2011; Sohn et al. 2013*).

46 Figures S8 and S9 show ALL forced simulations dry and wet regions when defined using
47 method 2. The top 4 panels show the percentage of years that each gridbox is defined as a
48 dry region or wet region averaged across all simulations and the bottom 4 panels show the
49 multi-model mean difference between the first 10 years and last 10 years. Figures S10 and
50 S11 shows the same results for RCP4.5 simulations for 2011 to 2035, illustrating that the
51 historical fingerprint results closely resembles a result using a near future fingerprint.

52 The purpose of examining the wet and dry regions in this way is to determine if they are
53 changing size. Figure S12 shows that in the tropics and subtropics any changes to the size of
54 the dry or wet regions for the GPCP dataset are generally small, (<10%). The ALL forced
55 and RCP4.5 models do not show a consistent change in the size of the dry and wet regions
56 for all simulations while the changes in the multi-model means are small for both (<5%).
57 Changes in the mid-latitudes are somewhat larger for both the observations and the models,
58 however, these are still less than the maximum observed year-to-year variation except in the
59 SH mid-latitudes, particularly in JAS where the expansion of the wet regions and reduction
60 of the dry regions is consistent with increasing precipitation at these latitudes.

61 *c. Observed and modeled changes in precipitation*

62 Figures S13 and S14 show the observed and simulated changes in precipitation in the
63 dry and wet regions for land only and ocean only respectively. Comparison of the figures
64 shows that the pattern of dry gets drier, wet gets wetter in the tropics and subtropics is
65 more consistent over ocean than land.

66 Long term trends in satellite data are still considered uncertain. To explore data uncer-
67 tainty to some extent, we compare changes over land with two station-based observational
68 datasets, GPCC and CRU, where both are masked to the wet and dry regions of GPCP
69 (Figure S15). The sign of the changes for GPCC and CRU generally match those of GPCP,
70 with GPCC (which is used to calibrate GPCP), more consistent than CRU.

71 Figure S16 shows the seasonal precipitation for the GPCP, GPCC and CRU datasets for
72 the Northern Hemisphere high latitudes for the years 1988-2010. The timeseries are similar
73 for all three datasets over land, with no large change in precipitation over this period. While
74 this is unsurprising given that in-situ data are used to cross calibrate satellite data (*Adler*
75 *et al.* 2003), it shows that trends are well constrained by stations.

77 Figure S17 shows the scaling factors for the combined fingerprint of the wet and dry
78 regions in all seasons for ALL, GHG, RCP4.5 and NAT forcing for the precipitation changes
79 shown in Figures 2, S13 and S14. Figure S18 shows the scaling factors when the influence of
80 ENSO is not removed from the observations, the detection results are the same except for
81 ALL forcing for land+ocean. The results for GHG and RCP4.5 are similar to those of ALL
82 forcing while NAT forcing is not detected (i.e. the 90% confidence interval includes zero).
83 Figure S19 shows the scaling factors for the dry and wet regions separately. For the wet
84 only regions, both GHG and NAT only forcing are detected. Combining the GHG and NAT
85 fingerprints in the 2-signal analysis shows that only GHG forcing is detected when the finger-
86 print contains both the wet and dry regions. The aerosol affects on precipitation are highly
87 uncertain and there were not enough simulations for anthropogenic only or anthropogenic
88 aerosol only to derive fingerprints with suitably a low signal signal-to-noise ratio.

89 Figure S20 shows the scaling factors for the control simulations. These show that there
90 is no bias introduced by the method of selecting the dry and wet regions that leads to false
91 detection results.

92

93 REFERENCES

- 94 Adler, R., et al. (2003), The version 2 global precipitation climatology project (gpcp) monthly
95 precipitation analysis (1979-present), *J. Hydrometeor.*, *4*, 1147–1167.
- 96 Gu, G., R. F. Adler, G. J. Huffman, and S. Curtis (2007), Tropical rainfall variability on
97 interannual-to-interdecadal and longer time scales derived from the gpcp monthly product,
98 *J. Climate*, *20*(15), 4033–4046, doi:10.1175/JCLI4227.1.

- 99 Kenyon, J., and G. Hegerl (2010), Influence of modes of climate variability on global precip-
100 itation extremes., *J. Clim.*, *23*, 6248–6262.
- 101 Merrifield, M. A. (2011), A shift in western tropical pacific sea level trends during the 1990s,
102 *J. Clim.*, *24*(15), 4126–4138.
- 103 Morice, C.P., J.J. Kennedy, N.A. Rayner, and P.D. Jones, 2012: Quantifying uncertainties
104 in global and regional temperature change using an ensemble of observational estimates:
105 the HadCRUT4 dataset. *J. Geophys. Res.*, *117*, D08101, doi:10.1029/2011JD017187.
- 106 Sohn, B., S.-W. Yeh, J. Schmetz, and H.-J. Song (2013), Observational evidences of walker
107 circulation change over the last 30years contrasting with gcm results, *Clim. Dyn.*, *40*(7-8),
108 1721–1732.
- 109 Wolter, K., and M. S. Timlin (2011), El Nino/Southern Oscillation behaviour since 1871
110 as diagnosed in an extended multivariate ENSO index (MEI.ext)., *Intl. J. Climatol.*, *31*,
111 1074–1087.

112 **List of Tables**

113 1 List of modelling groups and models used in this analysis

7

TABLE 1. List of modelling groups and models used in this analysis

<i>InstituteID</i>	<i>ModelName</i>	<i>Forcing(no.ofsims)</i>
CCCMA	CanESM2	GHG(5), NAT(5),CNT(2), RCP4.5(5)
CNRM-CERFACS	CNRM-CM5	ALL(5), GHG(5), NAT(5), CNT(1)
NASA GISS	GISS-E2-H	ALL(5), GHG(5), NAT(5), CNT(2)
NASA GISS	GISS-E2-R	ALL(5), GHG(5), NAT(5), CNT(2), RCP4.5(3)
MOHC	HadGEM2-ES	GHG(4), NAT(4), CNT(1), RCP4.5(3)
INM	INM-CM4	CNT(1), RCP4.5(1)
IPSL	IPSL-CM5A-LR	GHG(3), NAT(3), CNT(1)
NCC	NorESM1-M	ALL(3), GHG(1), NAT(1), CNT(1), RCP4.5(1)
CSIRO-QCCCE	CSIRO-Mk3.6.0	GHG(5), NAT(5), CNT(1), RCP4.5(1)
NCAR	CCSM4	RCP4.5(5), CNT(1)
MRI	MRI-CGCM3	ALL(5), RCP4.5(1)
EC-EARTH	EC-EARTH	ALL(4)
MIROC	MIROC5	ALL(3), RCP4.5(3)
MIROC	MIROC-ESM	RCP4.5(1)
MIROC	MIROC-ESM-CHEM	RCP4.5(1)
MIROC	MIROC4H	RCP4.5(3)
MPI-M	MPI-ESM-LR	RCP4.5(3)

114 List of Figures

- 115 S1 (a) GPCP monthly mean tropical precipitation (mm per day) in the Northern
116 and Southern Hemispheres averaged over years 1988-2010. (b) HadCRUT4
117 annual global mean near surface temperature anomalies (w.r.t. 1961-1990)
118 (Morice et al. 2012). 14
- 119 S2 GPCP seasonal precipitation for the years 1988-2010 for the dry and wet
120 regions in the tropics and subtropics. To ensure that the OND and JFM
121 seasons are consistent, OND is taken from the previous year (i.e. 1987-2009). 15
- 122 S3 As Figure S2 but with the influence of ENSO removed. 16
- 123 S4 As Figure 1 in the body of paper but for all seasons. GPCP dry regions for
124 OND, JFM, AMJ and JAS for 1988 to 2010 using method 1 (OND is 1987-
125 2009). TOP FOUR PANELS give the percentage of years each grid box is
126 defined as a dry region. LOWER FOUR PANELS show difference between
127 first 10 years and last 10 years (i.e. percentage of years wet in 2001-2010
128 minus 1988-1997), only grid boxes where the change is not zero are plotted.
129 ENSO is removed from observations. 17
- 130 S5 As Figure 1 in the body of paper but for wet regions for all seasons. GPCP
131 wet regions for OND, JFM, AMJ and JAS for 1988 to 2010 using method
132 1 (OND is 1987-2009). TOP FOUR PANELS give the percentage of years
133 each grid box is defined as a wet region. LOWER FOUR PANELS show
134 difference between first 10 years and last 10 years (i.e. percentage of years
135 wet in 2001-2010 minus 1988-1997), only grid boxes where the change is not
136 zero are plotted. ENSO is removed from observations. 18

137 S6 As Figure 1 in the body of paper but using method 2 for all seasons. GPCP
138 dry regions for OND, JFM, AMJ and JAS for 1988 to 2010 using method
139 2 (OND is 1987-2009). TOP FOUR PANELS give the percentage of years
140 each grid box is defined as a dry region. LOWER FOUR PANELS show
141 difference between first 10 years and last 10 years (i.e. percentage of years
142 dry in 2001-2010 minus 1988-1997), only grid boxes where the change is not
143 zero are plotted. ENSO is removed from observations. 19

144 S7 As Figure 1 in the body of paper but using method 2 for the wet regions
145 for all seasons. GPCP wet regions for OND, JFM, AMJ and JAS for 1988
146 to 2010 using method 2 (OND is 1987-2009). TOP FOUR PANELS give
147 the percentage of years each grid box is defined as a wet region. LOWER
148 FOUR PANELS show difference between first 10 years and last 10 years (i.e.
149 percentage of years wet in 2001-2010 minus 1988-1997), only grid boxes where
150 the change is not zero are plotted. ENSO is removed from observations. 20

151 S8 Shows similar results to Figure 1 in body of the paper for the models. ALL
152 forced models mean dry regions for OND, JFM, AMJ and JAS for 1988 to
153 2010 using method 2 (OND is 1987-2009). TOP FOUR PANELS give the
154 multi-model mean percentage of years each grid box is defined as a dry region.
155 LOWER FOUR PANELS show difference between first 10 years and last 10
156 years (i.e. percentage of years dry in 2001-2010 minus 1988-1997) averaged
157 for all simulations, only grid boxes where the change is not zero are plotted. 21

158 S9 Shows similar results to Figure 1 in body of the paper for the models. ALL
159 forced models mean wet regions for OND, JFM, AMJ and JAS for 1988 to
160 2010 using method 2 (OND is 1987-2009). TOP FOUR PANELS give the
161 multi-model mean percentage of years each grid box is defined as a wet region.
162 LOWER FOUR PANELS show difference between first 10 years and last 10
163 years (i.e. percentage of years wet in 2001-2010 minus 1988-1997) averaged
164 for all simulations, only grid boxes where the change is not zero are plotted. 22

165 S10 Shows similar results to Figure 1 in body of the paper for the models. RCP4.5
166 forced models mean dry regions for OND, JFM, AMJ and JAS for 2011 to
167 2035 using method 2 (OND is 2010-2034). TOP FOUR PANELS give the
168 multi-model mean percentage of years each grid box is defined as a dry region.
169 LOWER FOUR PANELS show difference between first 10 years and last 10
170 years (i.e. percentage of years dry in 2026-2035 minus 2011-2020), only grid
171 boxes where the change is not zero are plotted. 23

172 S11 Shows similar results to Figure 1 in body of the paper for the models. RCP4.5
173 forced models mean wet regions for OND, JFM, AMJ and JAS for 2011 to
174 2035 using method 2 (OND is 2010-2034). TOP FOUR PANELS give the
175 multi-model mean percentage of years each grid box is defined as a wet region.
176 LOWER FOUR PANELS show difference between first 10 years and last 10
177 years (i.e. percentage of years wet in 2026-2035 minus 2011-2020), only grid
178 boxes where the change is not zero are plotted. 24

179 S12 Changing size of size of dry (TOP FOUR PANELS) and wet (LOWER FOUR
180 PANELS) regions using method 2, i.e. mean number of grid boxes for 2001-
181 2010 minus mean number of grid boxes for 1988-1997 (OND uses 1987-2009),
182 as percentage of mean number of grid boxes in all years in the dry/wet regions.
183 ENSO is removed from observations. 25

184 S13 As Figure 2 in the body of paper but for land only. Observed and modelled
185 zonal mean trends (% per year) in the dry (TOP FOUR PANELS) and wet
186 (LOWER FOUR PANELS) regions over land for 1988 to 2010 (OND is 1987-
187 2009). Note GPCP changes are plotted on a larger scale and the influence of
188 ENSO is removed from observations. The colored bars give the multi-model
189 mean trends for the ALL, GHG and rcp4.5 simulations. The orange shading
190 show where GPCP, ALL and rcp4.5 all give negative trends and the blue
191 shading shows where they give positive trends. 26

192 S14 As Figure 2 in the body of paper but for ocean only. Observed and modelled
193 zonal mean trends (% per year) in the dry (TOP FOUR PANELS) and wet
194 (LOWER FOUR PANELS) regions over the ocean for 1988 to 2010 (OND
195 is 1987-2009). Note GPCP changes are plotted on a larger scale and the
196 influence of ENSO is removed from observations. The colored bars give the
197 multi-model mean trends for the ALL, GHG and rcp4.5 simulations. The
198 orange shading show where GPCP, ALL and rcp4.5 all give negative trends
199 and the blue shading shows where they give positive trends. 27

200 S15 As Figure 2 in body of paper for 3 different observational datasets for land
201 only. Robustness of observed changes over land for 1988 to 2010 (OND is
202 1987-2009). Observed and multi-model mean zonal mean trends (MM) (% per
203 year) in the dry (TOP FOUR PANELS) and wet (LOWER FOUR PANELS)
204 regions over land for the GPCP, GPCC and CRU observations datasets where
205 the GPCC and CRU datasets were masked to match the dry and wet regions in
206 the GPCP dataset. The orange shading shows where the changes for GPCP,
207 GPCC and CRU are all negative and blue were they are all positive. The
208 changes for all land are also shown for all 3 observation datasets ($GPCP_{al}$,
209 $GPCC_{al}$ and CRU_{al}) and for all land+ocean for GPCP ($GPCP_{alo}$). This
210 influence of ENSO is removed from observations. 28

211 S16 Observed land precipitation in the Northern Hemisphere high latitudes (60N
212 to 90N) for 1988 to 2010 (OND is 1987-2009) for 3 observational datasets,
213 GPCP, GPCC and CRU and ocean for GPCP. 29

214 S17 Detection and attribution results: As Figure 3 upper panel but using fin-
215 gerprints for individual forcings. Scaling factors for the wet and dry regions
216 combined for ALL, GHG, NAT and RCP4.5 simulations with ENSO removed
217 from observations Crosses show the 'best-guess' scaling factor for the multi-
218 model mean, thick lines are the 90% confidence interval for the raw model
219 variance added as noise and thin lines are the 90% confidence interval for
220 double the variance. L+O is land+ocean for the GPCP dataset. Note differ-
221 ent scale used for NAT forcing. The residual consistency test is passed for all
222 forcings for double the model variance. 30

223 S18 Detection and attribution results: As Figure 3 upper panel and Figure S17
224 using fingerprints for individual forcings but with ENSO not removed from
225 observations. Scaling factors for the wet and dry regions combined for ALL,
226 GHG, NAT and RCP4.5 simulations. Crosses show the 'best-guess' scaling
227 factor for the multi-model mean, thick lines are the 90% confidence interval for
228 the raw model variance added as noise and thin lines are the 90% confidence
229 interval for double the variance. L+O is land+ocean for the GPCP dataset.
230 Note different scale used for NAT forcing. The residual consistency test is
231 passed for all forcings for double the model variance. 31

232 S19 Detection and attribution results: As Figure 3 upper panel but using fin-
233 gerprints for individual forcings and wet and dry regions separately. Scaling
234 factor for the ALL, GHG, NAT, and RCP4.5 simulations for wet and dry
235 regions separately with ENSO removed from observations. Crosses show the
236 'best-guess' scaling factor for the multi-model mean, thick lines are the 90%
237 confidence interval for the raw model variance added as noise and thin lines
238 are the 90% confidence interval for double the variance. Note different scale
239 used for NAT forcing. The residual consistency test is passed for all forcings
240 for double the model variance. 32

241 S20 Detection and attribution results: As Figure 3 upper panel but using finger-
242 prints for control only simulations. UPPER PANEL Scaling factors for the
243 control simulations fingerprint for combined dry and wet regions for land+ocean,
244 ocean only and land only for the 3 observations datasets GPCP, GPCC and
245 CRU and LOWER PANEL individual dry and wet regions for land+ocean
246 for the GPCP dataset. This shows that no artificial trends are introduced by
247 the analysis method that produce false detection if forcing. 33

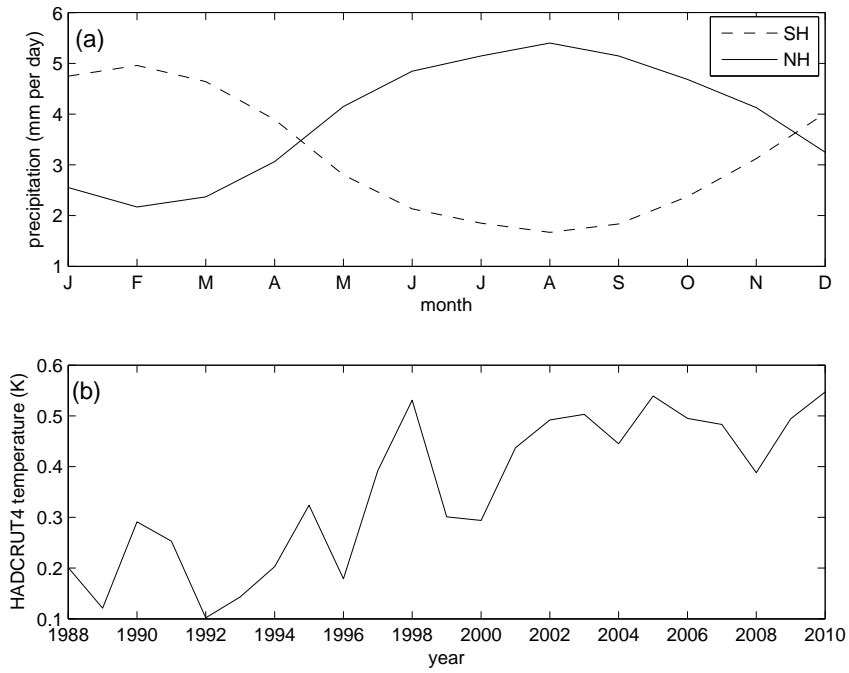


FIG. S1. (a) GPCP monthly mean tropical precipitation (mm per day) in the Northern and Southern Hemispheres averaged over years 1988-2010. (b) HadCRUT4 annual global mean near surface temperature anomalies (w.r.t. 1961-1990) (Morice et al. 2012).

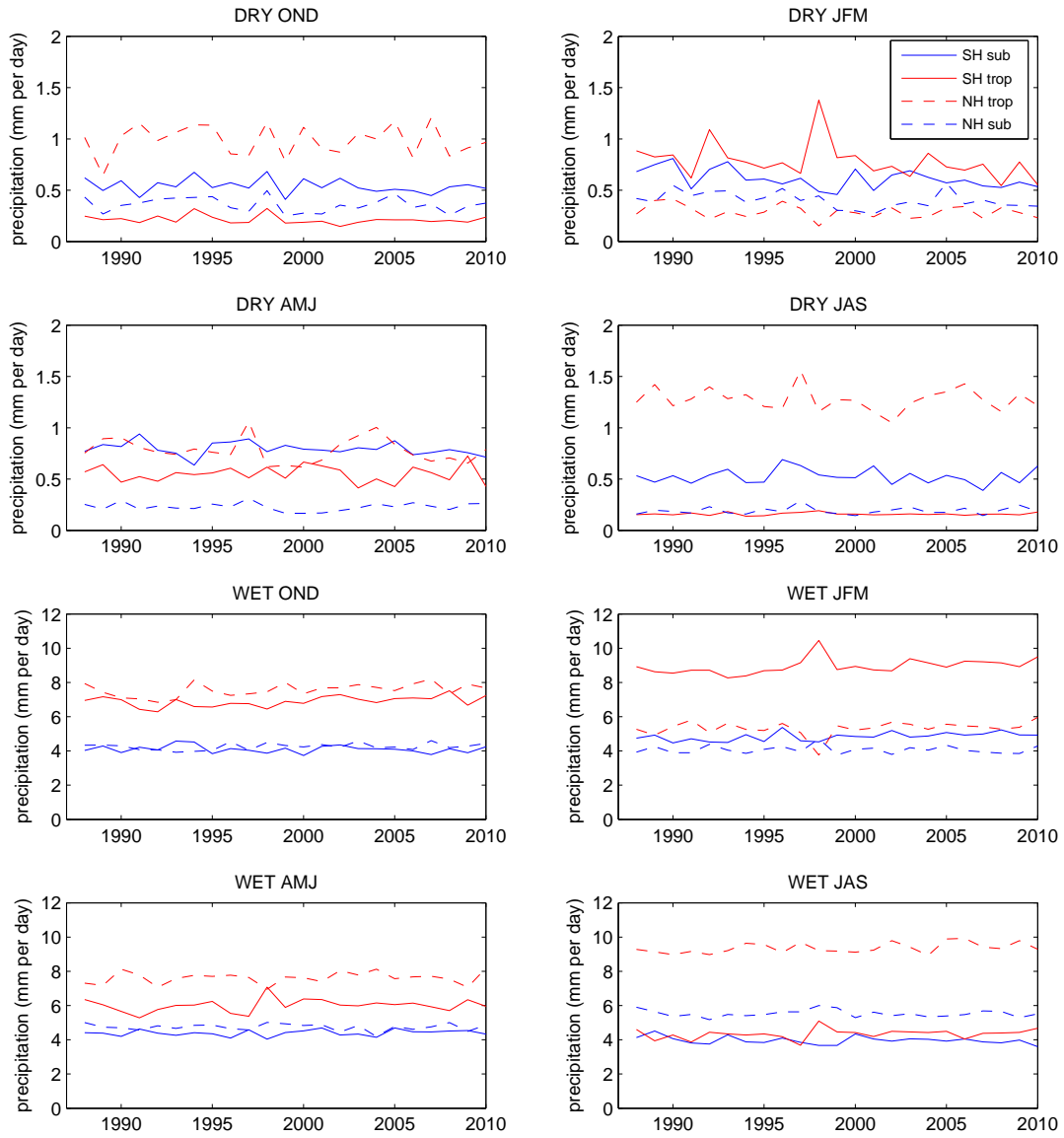


FIG. S2. GPCP seasonal precipitation for the years 1988-2010 for the dry and wet regions in the tropics and subtropics. To ensure that the OND and JFM seasons are consistent, OND is taken from the previous year (i.e. 1987-2009).

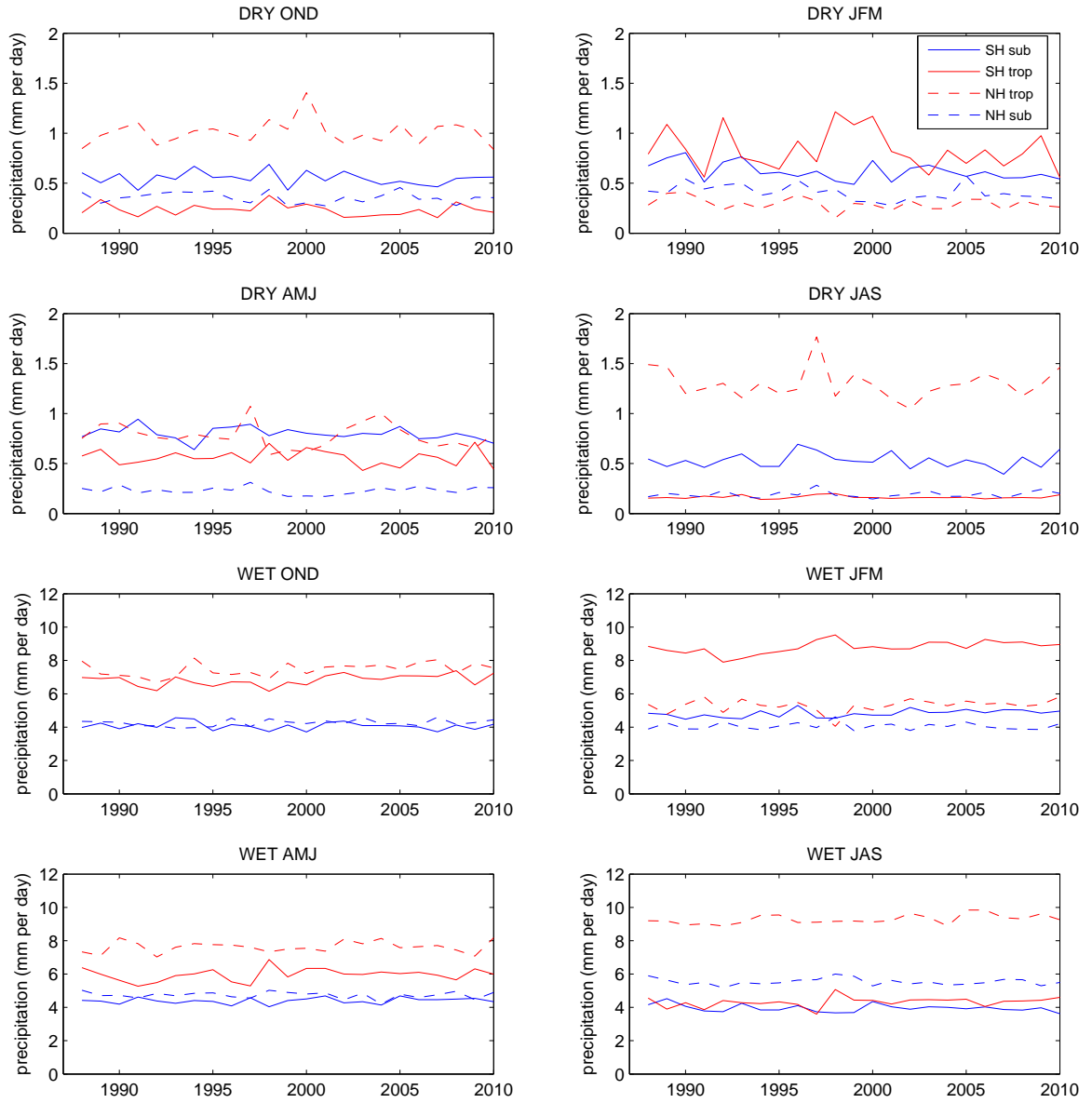


FIG. S3. As Figure S2 but with the influence of ENSO removed.

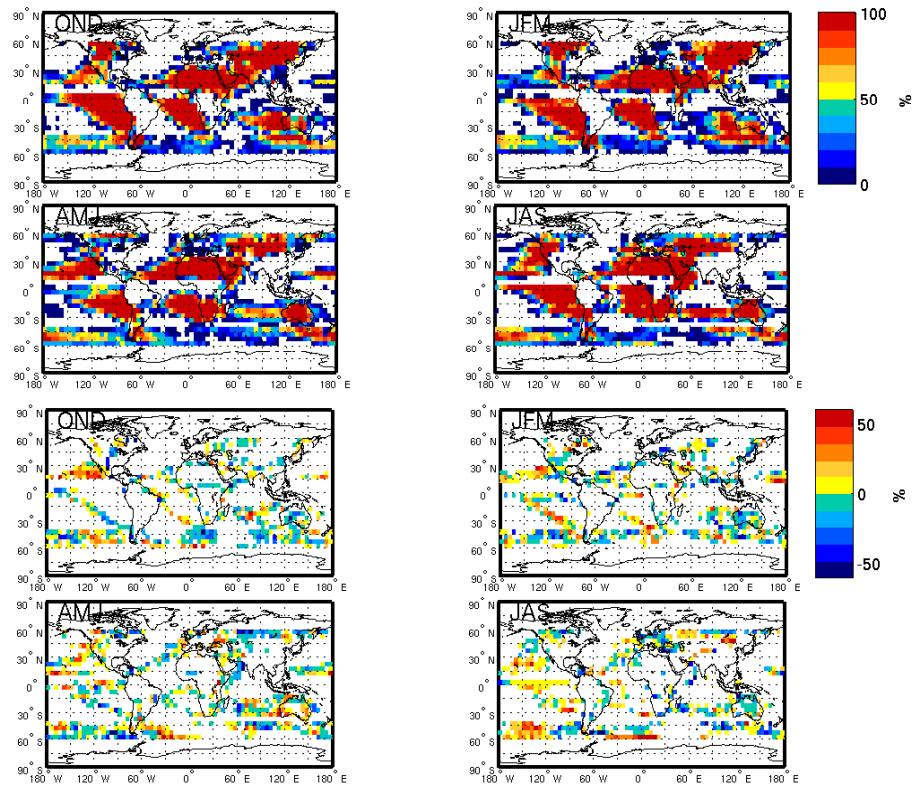


FIG. S4. As Figure 1 in the body of paper but for all seasons. GPCP dry regions for OND, JFM, AMJ and JAS for 1988 to 2010 using method 1 (OND is 1987-2009). TOP FOUR PANELS give the percentage of years each gridbox is defined as a dry region. LOWER FOUR PANELS show difference between first 10 years and last 10 years (i.e. percentage of years wet in 2001-2010 minus 1988-1997), only gridboxes where the change is not zero are plotted. ENSO is removed from observations.

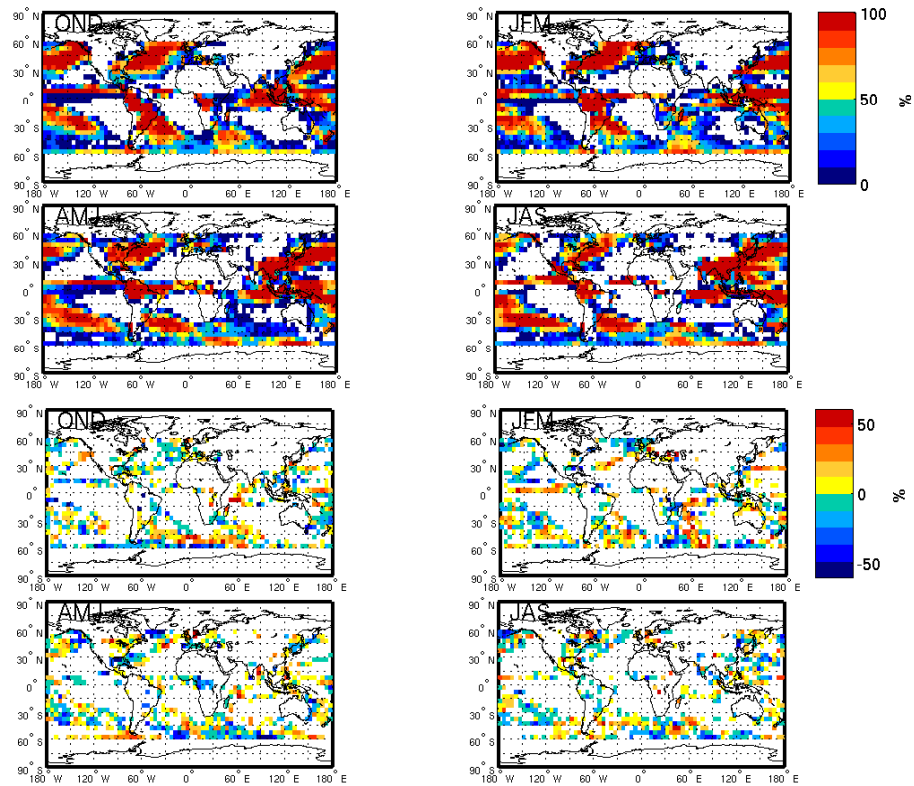


FIG. S5. As Figure 1 in the body of paper but for wet regions for all seasons. GPCP wet regions for OND, JFM, AMJ and JAS for 1988 to 2010 using method 1 (OND is 1987-2009). TOP FOUR PANELS give the percentage of years each gridbox is defined as a wet region. LOWER FOUR PANELS show difference between first 10 years and last 10 years (i.e. percentage of years wet in 2001-2010 minus 1988-1997), only gridboxes where the change is not zero are plotted. ENSO is removed from observations.

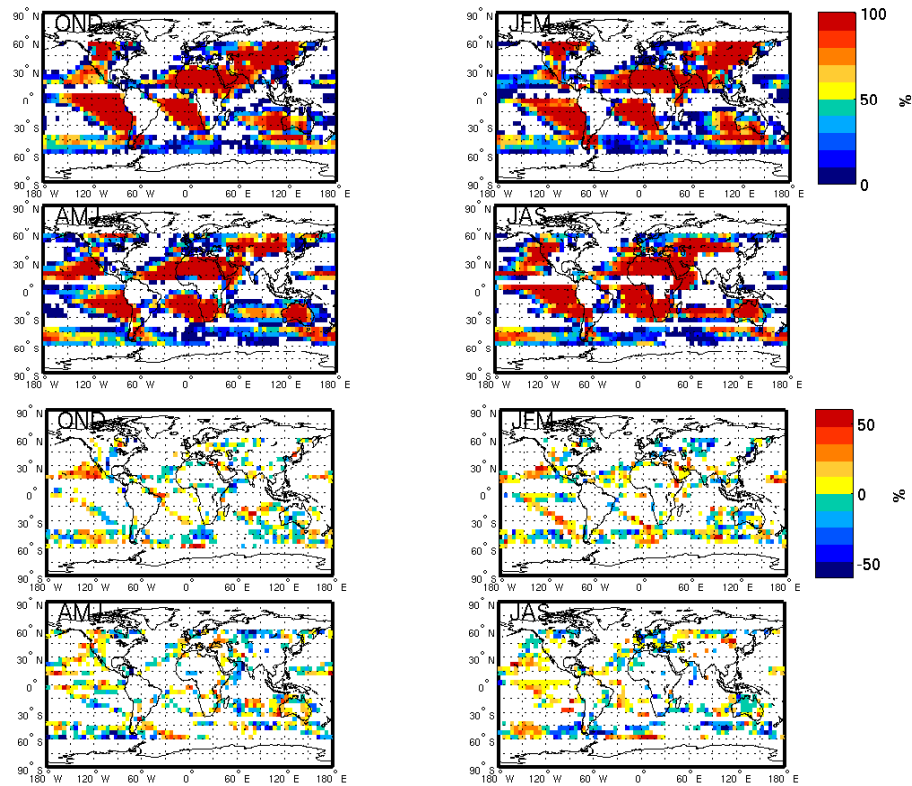


FIG. S6. As Figure 1 in the body of paper but using method 2 for all seasons. GPCP dry regions for OND, JFM, AMJ and JAS for 1988 to 2010 using method 2 (OND is 1987-2009). TOP FOUR PANELS give the percentage of years each gridbox is defined as a dry region. LOWER FOUR PANELS show difference between first 10 years and last 10 years (i.e. percentage of years dry in 2001-2010 minus 1988-1997), only gridboxes where the change is not zero are plotted. ENSO is removed from observations.

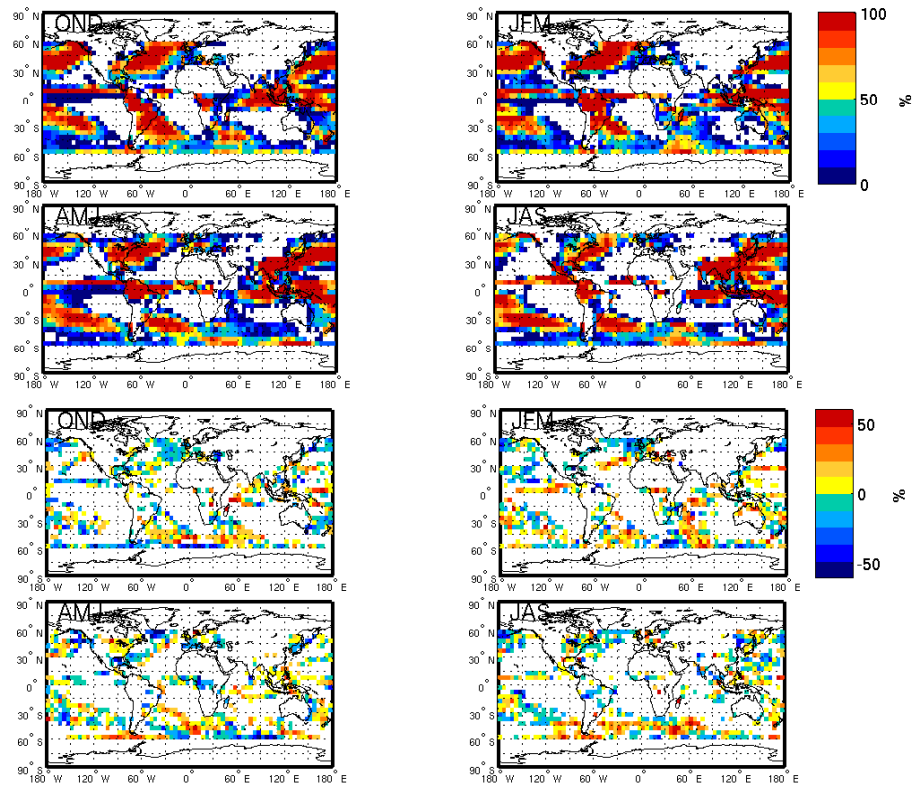


FIG. S7. As Figure 1 in the body of paper but using method 2 for the wet regions for all seasons. GPCP wet regions for OND, JFM, AMJ and JAS for 1988 to 2010 using method 2 (OND is 1987-2009). TOP FOUR PANELS give the percentage of years each gridbox is defined as a wet region. LOWER FOUR PANELS show difference between first 10 years and last 10 years (i.e. percentage of years wet in 2001-2010 minus 1988-1997), only gridboxes where the change is not zero are plotted. ENSO is removed from observations.

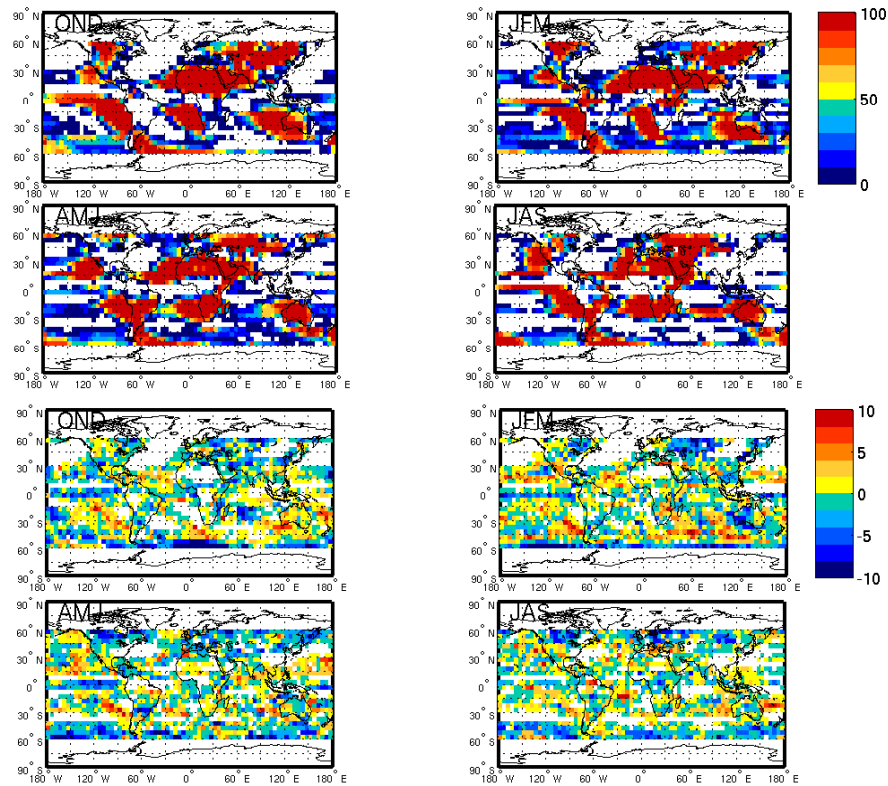


FIG. S8. Shows similar results to Figure 1 in body of the paper for the models. ALL forced models mean dry regions for OND, JFM, AMJ and JAS for 1988 to 2010 using method 2 (OND is 1987-2009). TOP FOUR PANELS give the multi-model mean percentage of years each gridbox is defined as a dry region. LOWER FOUR PANELS show difference between first 10 years and last 10 years (i.e. percentage of years dry in 2001-2010 minus 1988-1997) averaged for all simulations, only gridboxes where the change is not zero are plotted.

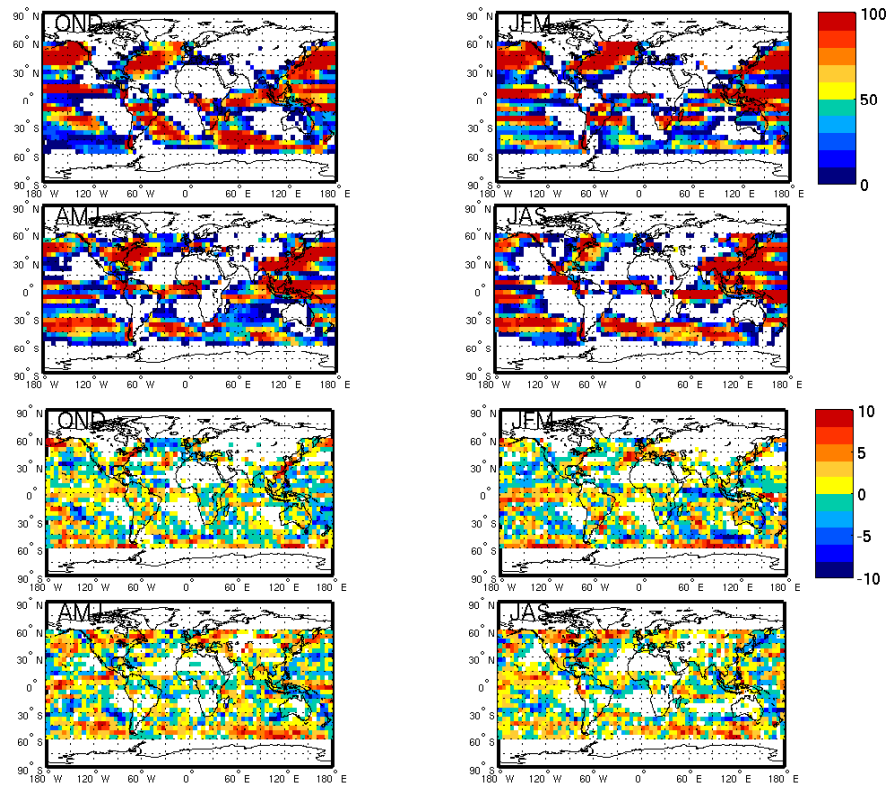


FIG. S9. Shows similar results to Figure 1 in body of the paper for the models. ALL forced models mean wet regions for OND, JFM, AMJ and JAS for 1988 to 2010 using method 2 (OND is 1987-2009). TOP FOUR PANELS give the multi-model mean percentage of years each gridbox is defined as a wet region. LOWER FOUR PANELS show difference between first 10 years and last 10 years (i.e. percentage of years wet in 2001-2010 minus 1988-1997) averaged for all simulations, only gridboxes where the change is not zero are plotted.

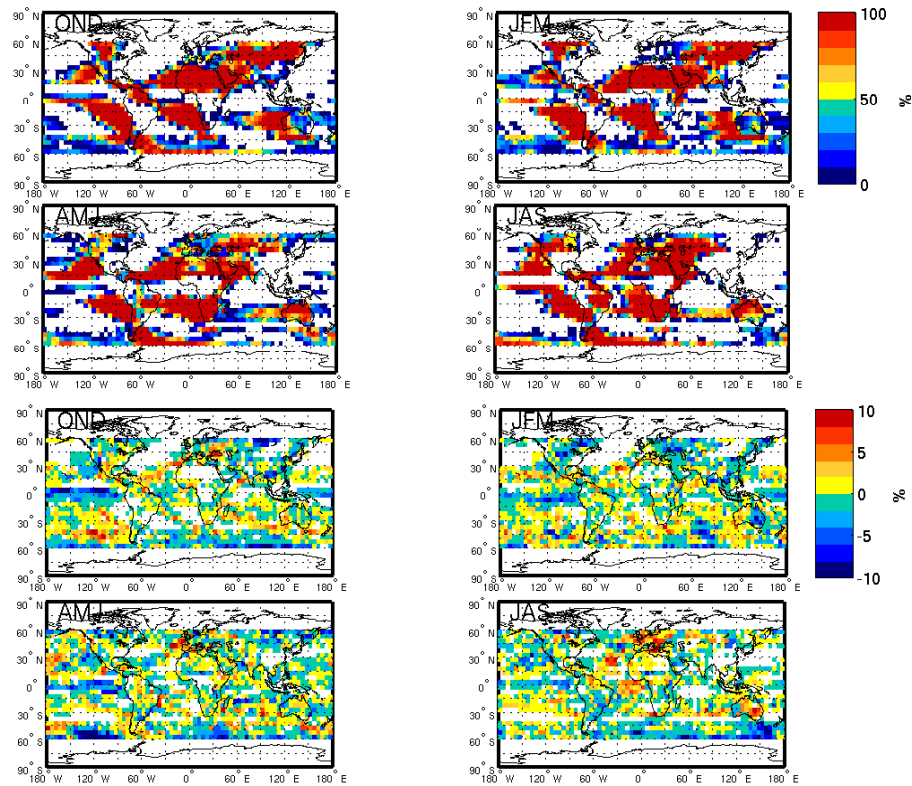


FIG. S10. Shows similar results to Figure 1 in body of the paper for the models. RCP4.5 forced models mean dry regions for OND, JFM, AMJ and JAS for 2011 to 2035 using method 2 (OND is 2010-2034). TOP FOUR PANELS give the multi-model mean percentage of years each gridbox is defined as a dry region. LOWER FOUR PANELS show difference between first 10 years and last 10 years (i.e. percentage of years dry in 2026-2035 minus 2011-2020), only gridboxes where the change is not zero are plotted.

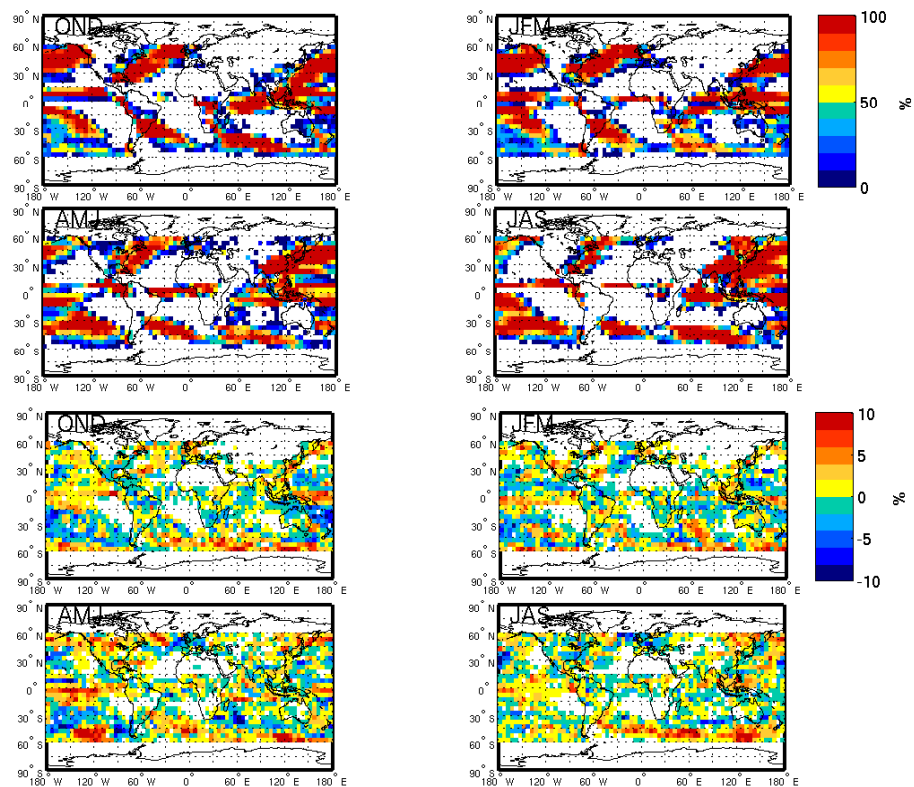


FIG. S11. Shows similar results to Figure 1 in body of the paper for the models. RCP4.5 forced models mean wet regions for OND, JFM, AMJ and JAS for 2011 to 2035 using method 2 (OND is 2010-2034). TOP FOUR PANELS give the multi-model mean percentage of years each gridbox is defined as a wet region. LOWER FOUR PANELS show difference between first 10 years and last 10 years (i.e. percentage of years wet in 2026-2035 minus 2011-2020), only gridboxes where the change is not zero are plotted.

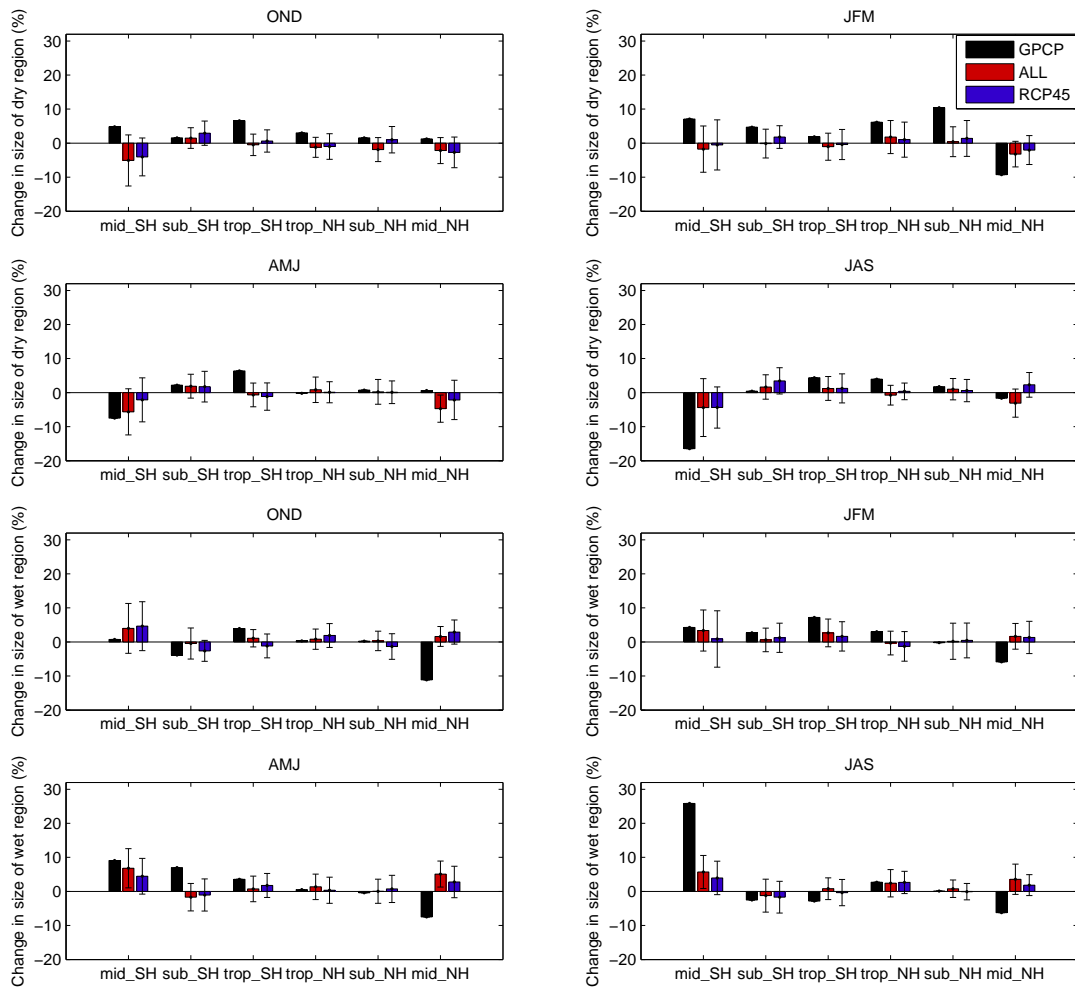


FIG. S12. Changing size of size of dry (TOP FOUR PANELS) and wet (LOWER FOUR PANELS) regions using method 2, i.e. mean number of grid boxes for 2001-2010 minus mean number of gridboxes for 1988-1997 (OND uses 1987-2009), as percentage of mean number of gridboxes in all years in the dry/wet regions. ENSO is removed from observations.

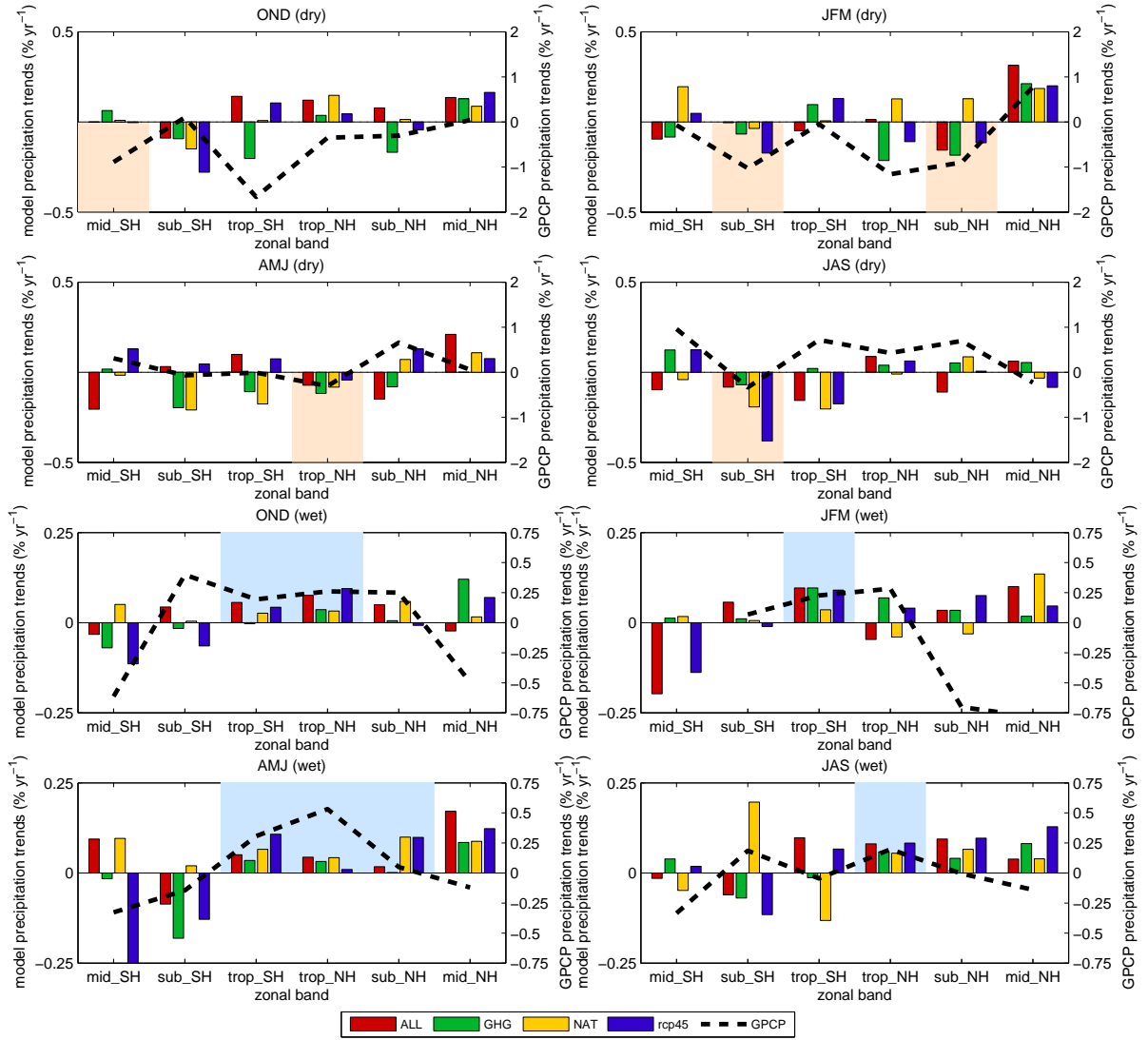


FIG. S13. As Figure 2 in the body of paper but for land only. Observed and modelled zonal mean trends ($\%$ per year) in the dry (TOP FOUR PANELS) and wet (LOWER FOUR PANELS) regions over land for 1988 to 2010 (OND is 1987-2009). Note GPCP changes are plotted on a larger scale and the influence of ENSO is removed from observations. The colored bars give the multi-model mean trends for the ALL, GHG and rcp4.5 simulations. The orange shading show where GPCP, ALL and rcp4.5 all give negative trends and the blue shading shows where they give positive trends.

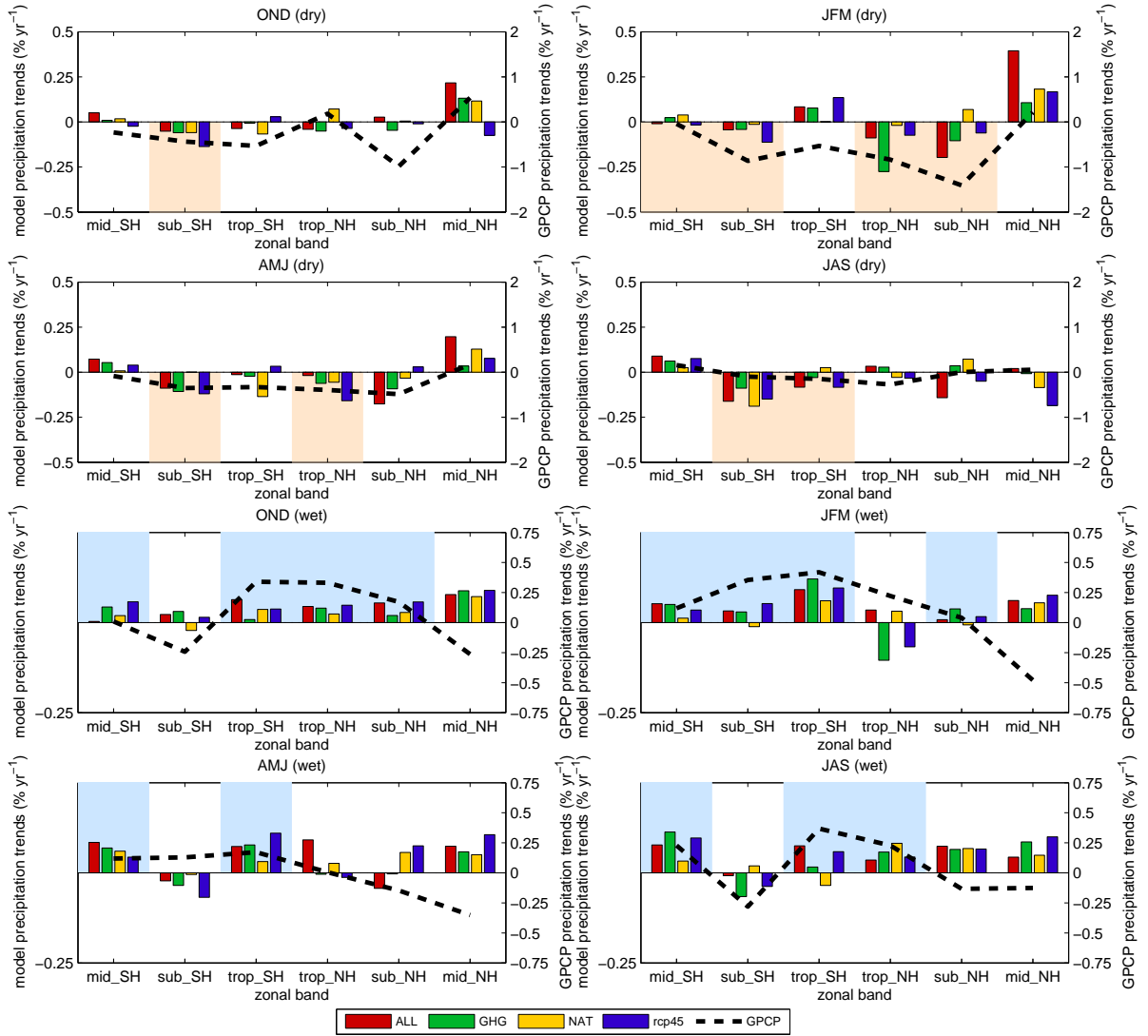


FIG. S14. As Figure 2 in the body of paper but for ocean only. Observed and modelled zonal mean trends (% per year) in the dry (TOP FOUR PANELS) and wet (LOWER FOUR PANELS) regions over the ocean for 1988 to 2010 (OND is 1987-2009). Note GPCP changes are plotted on a larger scale and the influence of ENSO is removed from observations. The colored bars give the multi-model mean trends for the ALL, GHG and rcp4.5 simulations. The orange shading show where GPCP, ALL and rcp4.5 all give negative trends and the blue shading shows where they give positive trends.

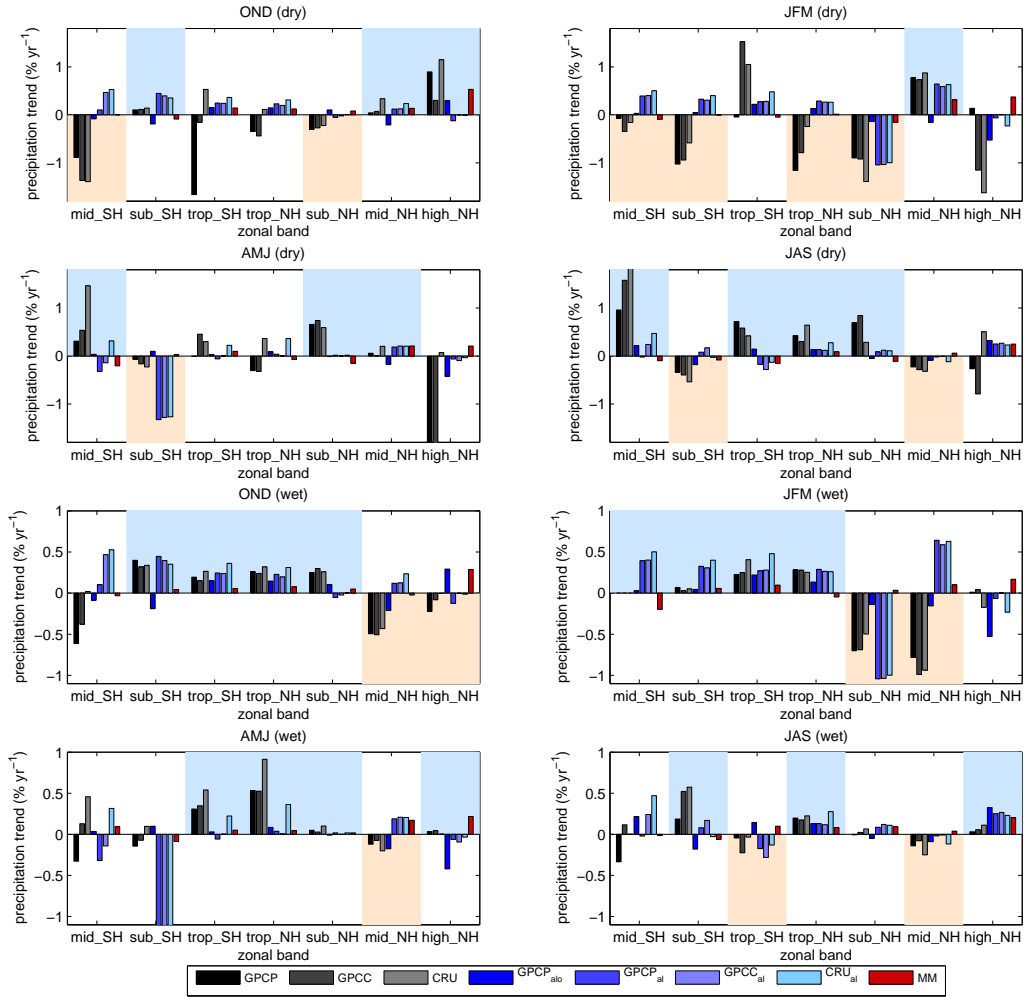


FIG. S15. As Figure 2 in body of paper for 3 different observational datasets for land only. Robustness of observed changes over land for 1988 to 2010 (OND is 1987-2009). Observed and multi-model mean zonal mean trends (MM) (% per year) in the dry (TOP FOUR PANELS) and wet (LOWER FOUR PANELS) regions over land for the GPCP, GPCCC and CRU observations datasets where the GPCCC and CRU datasets were masked to match the dry and wet regions in the GPCP dataset. The orange shading shows where the changes for GPCP, GPCCC and CRU are all negative and blue were they are all positive. The changes for all land are also shown for all 3 observation datasets ($GPCP_{al}$, $GPCCC_{al}$ and CRU_{al}) and for all land+ocean for GPCP ($GPCP_{alo}$). This influence of ENSO is removed from observations.

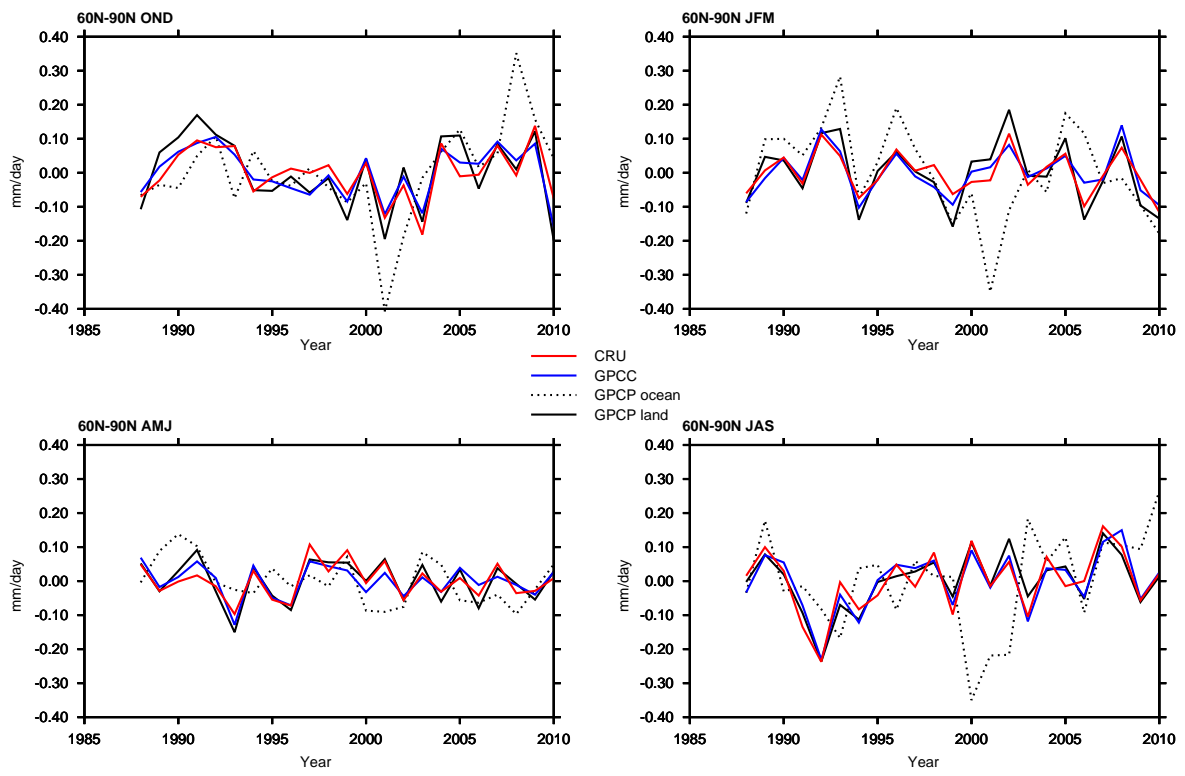


FIG. S16. Observed land precipitation in the Northern Hemisphere high latitudes (60N to 90N) for 1988 to 2010 (OND is 1987-2009) for 3 observational datasets, GPCP, GPCP and CRU and ocean for GPCP.

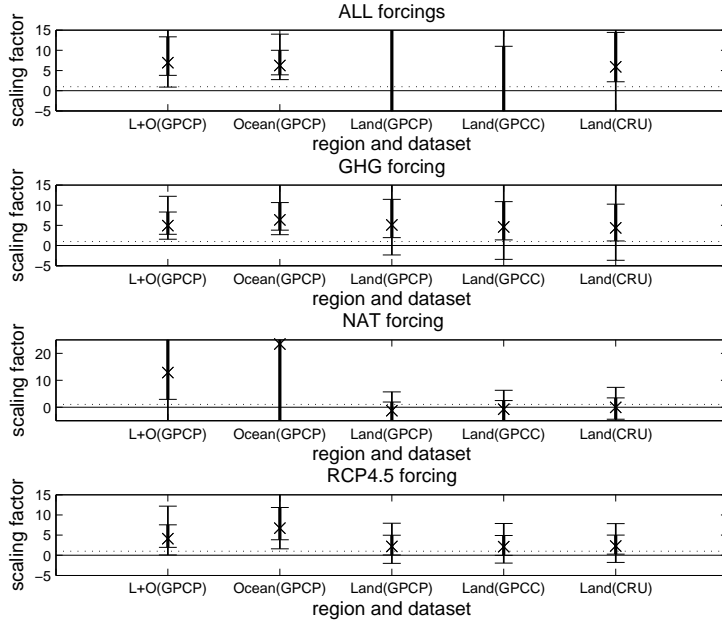


FIG. S17. Detection and attribution results: As Figure 3 upper panel but using fingerprints for individual forcings. Scaling factors for the wet and dry regions combined for ALL, GHG, NAT and RCP4.5 simulations with ENSO removed from observations. Crosses show the 'best-guess' scaling factor for the multi-model mean, thick lines are the 90% confidence interval for the raw model variance added as noise and thin lines are the 90% confidence interval for double the variance. L+O is land+ocean for the GPCP dataset. Note different scale used for NAT forcing. The residual consistency test is passed for all forcings for double the model variance.

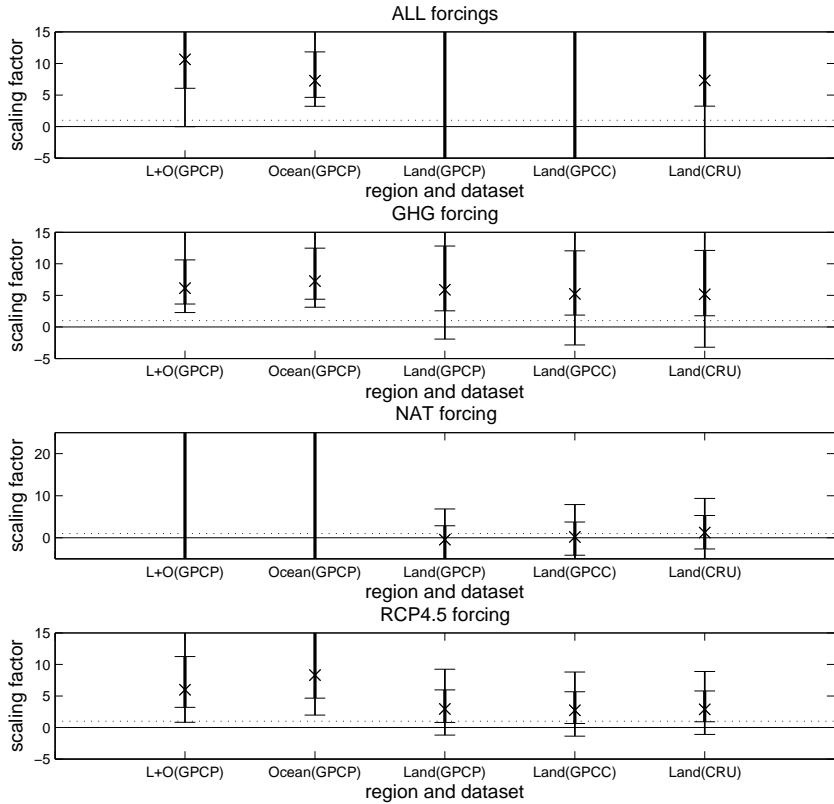


FIG. S18. Detection and attribution results: As Figure 3 upper panel and Figure S17 using fingerprints for individual forcings but with ENSO not removed from observations. Scaling factors for the wet and dry regions combined for ALL, GHG, NAT and RCP4.5 simulations. Crosses show the 'best-guess' scaling factor for the multi-model mean, thick lines are the 90% confidence interval for the raw model variance added as noise and thin lines are the 90% confidence interval for double the variance. L+O is land+ocean for the GPCP dataset. Note different scale used for NAT forcing. The residual consistency test is passed for all forcings for double the model variance.

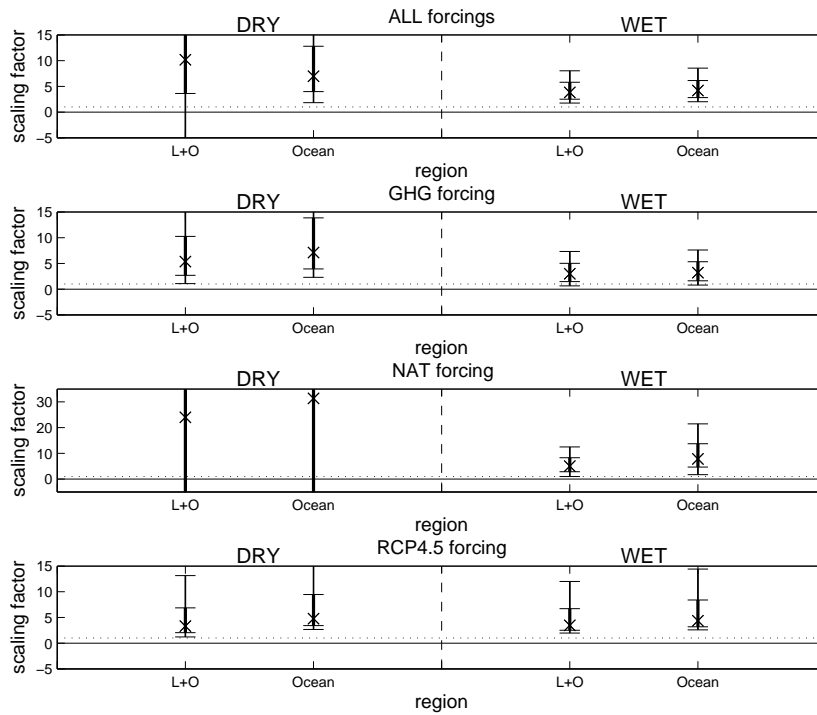


FIG. S19. Detection and attribution results: As Figure 3 upper panel but using fingerprints for individual forcings and wet and dry regions separately. Scaling factor for the ALL, GHG, NAT, and RCP4.5 simulations for wet and dry regions separately with ENSO removed from observations. Crosses show the 'best-guess' scaling factor for the multi-model mean, thick lines are the 90% confidence interval for the raw model variance added as noise and thin lines are the 90% confidence interval for double the variance. Note different scale used for NAT forcing. The residual consistency test is passed for all forcings for double the model variance.

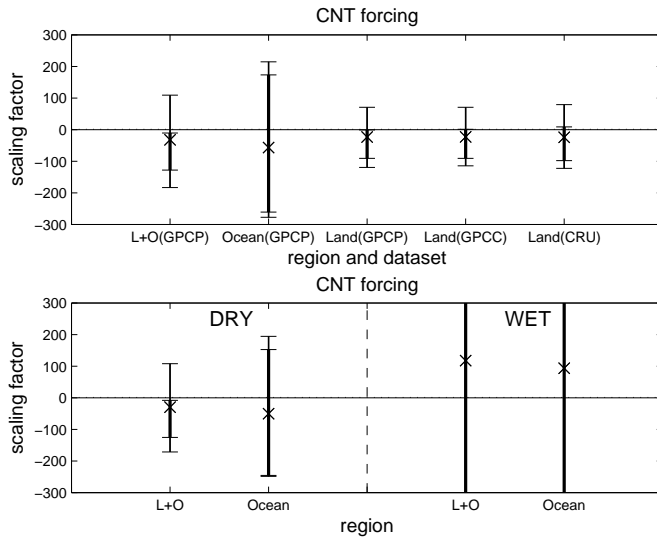


FIG. S20. Detection and attribution results: As Figure 3 upper panel but using fingerprints for control only simulations. UPPER PANEL Scaling factors for the control simulations fingerprint for combined dry and wet regions for land+ocean, ocean only and land only for the 3 observations datasets GPCP, GPCC and CRU and LOWER PANEL individual dry and wet regions for land+ocean for the GPCP dataset. This shows that no artificial trends are introduced by the analysis method that produce false detection if forcing.